Long-Horizon Robust Direct Model Predictive Control for Medium-Voltage Drives with Active Neutral-Point Potential Balancing

Andrei Tregubov
Faculty of Information Technology and Communication Sciences
Tampere University
Tampere, Finland
andrei.tregubov@tuni.fi

Petros Karamanakos
Faculty of Information Technology and Communication Sciences
Tampere University
Tampere, Finland
p.karamanakos@ieee.org

Ludovico Ortombina
Department of Industrial Engineering
University of Padua
Padua, Italy
ludovico.ortombina@unipd.it

***Abstract*—The paper presents a direct model predictive control algorithm for medium-voltage (MV) induction machines driven by three-level neutral-point-clamped (NPC) inverters that incorporates the neutral point potential balancing. For such nonlinear systems implementation of long horizons may be regarded as even a formidable task due to the high computational complexity. Nevertheless, this can be achieved with a modest calculation cost by decreasing the size of the underlying control optimization problem. Moreover, when assisted by a light estimation algorithm, the developed control scheme achieves a high level of robustness to variations in the motor parameters. The presented results demonstrate the effectiveness of the proposed method during steady-state and transient operating conditions.**

***Index Terms*—AC drives, medium-voltage (MV) drives, model predictive control (MPC), direct control, robust control**

I. Introduction

Three-level neutral-point-clamped (NPC) converters are a common choice in medium voltage (MV) drive applications due to the higher efficiency and better quality of the output current they offer in comparison to a two-level topology [1]. Such converters, however, require balancing of the neutral point (NP) potential to maintain equal distribution of the dc-link voltage across the upper and lower dc-link capacitors, see Fig. 1. To achieve this, several control approaches modify the voltage reference that is driven to a pulse width modulation (PWM) stage. For example, [2] uses a zero-sequence voltage injection into the modulating signal of a carrier-based PWM (CB-PWM) strategy. [3] exploits the redundancy in the voltage vectors that alter the NP current but do not affect the converter output voltage. In a similar way, [4] proposes a method to modify the application times of the redundant vectors utilized in space vector modulation (SVM).

However, the effectiveness of such techniques is often compromised at certain operating points associated with high modulation indices and low power factors [5], [6]. Another approach, suitable especially for low- or no-load operation, manipulates the line currents, but at the expense of an increased output current total harmonic distortion (THD) [7]. Thus, as can be understood, the NP potential balancing with linear control strategies is a non-trivial task that may result in complicated control designs, especially when various operating points are considered [8].

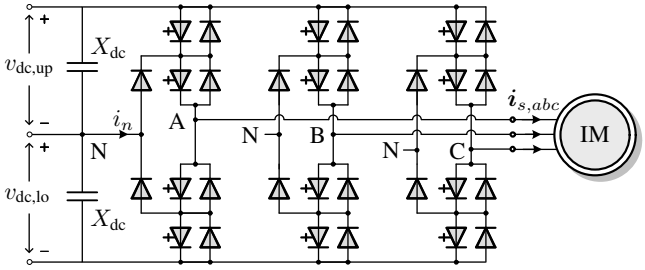

Fig. 1. Three-level NPC voltage-source inverter (VSI) driving an IM.

A simpler design perspective on the NP potential balancing is offered by model predictive control (MPC) because it is capable of handling multi-input multi-output (MIMO) systems, thus avoiding cascaded control loop structures. One of the subcategories of MPC—finite control set MPC (FCS-MPC), which is considered in this work—features control and modulation problem in one computational stage. As a result, the controller outputs the switching signals that are directly applied to the converter without a dedicated modulator, thus enabling very fast dynamic responses. In the framework of the said direct MPC approach, the problem of the NP potential balancing is addressed in [9], [10]. However, these works do not fully address the common drawbacks associated with FCS-MPC as discussed in the following.

As the computational complexity of FCS-MPC increases exponentially with the number of the prediction horizon steps, its real-time implementation poses significant challenges. Consequently, many works resort to the one-step prediction, thus not fully exploiting the potential performance benefits of FCS-MPC [11]. To keep the calculation complexity at bay, non-trivial prediction horizons [11]–[13], or more sophisticated solvers such as the sphere decoding algorithm (SDA) [14], [15] can be adopted. Although, the NP potential balancing is not considered in the said methods, their formulation can be modified to include the problem in the control objectives. For example, since the dynamics of the NP potential lead to a nonlinear prediction model, SDA cannot be directly used. To overcome this issue, in works [9], [10] SDA was modified to work with a linearized system model. Obtaining the latter, however, may be a computationally demanding task, if done in real time. Also,

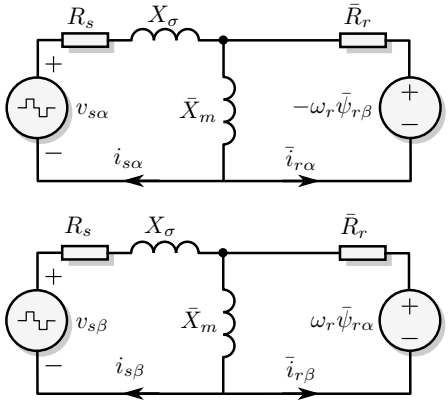

Fig. 2. Equivalent inverse-Γ model of an IM.

differences between the controller prediction model and the actual nonlinear system model are introduced with the linearization, what may compromise the system performance.

Besides the unmodeled or linearized dynamics, the performance of FCS-MPC may degrade due to changes in the system parameters. For example, variations in the resistances and inductors of an induction machine (IM) typically occur due to, e.g., changes in temperature or saturation of the magnetic material. Hence, MPC needs to be equipped with tools to account for any mismatches that negatively affect the controller performance. To this end, an external disturbance observer [16]–[18], or a system identification algorithm—either with full knowledge of the system [19] or without any dependency on it [20]—can be used. However, such methods tend to increase the complexity of the closed-loop controller design, often along with the computational burden. Considering that the latter needs to be kept relatively low such that the real-time implementation of long-horizon FCS-MPC is possible, such auxiliary tools should not add much computational overhead.

Motivated by the above, this paper proposes a long-horizon FCS-MPC that performs the active NP potential balancing for an MV IM driven by a three-level NPC converter. To this end, the objective function is complemented with a penalization of the NP potential deviation such that the reference tracking of all the controlled variables is achieved in one computational stage. To limit the calculation burden of the latter, the split prediction horizon is adopted in line with the method proposed in [13]. Moreover, the most crucial parameter deviations that affect the controller behavior are addressed with a refined estimation algorithm adopted from [21].

II. System Modeling

The mathematical model for the chosen case study, which is shown in Fig. 1, is derived in the following using per unit (p.u.) quantities. To this end, the stationary frame is adopted, and the subscripts for variables in the $\alpha\beta$-plane are dropped. The mapping from the abc- into the $\alpha\beta$-plane and vice versa is done with the reduced Clarke transformation matrix $\widetilde{\boldsymbol{K}}$ and its pseudo-inverse $\widetilde{\boldsymbol{K}}^{-1}$, respectively [22, Chapter 2.1].

In this work, the sum of the voltages across the lower $v_{\text{dc,lo}}$ and upper $v_{\text{dc,up}}$ dc-link capacitors X_{dc} comprises the constant dc-link voltage

$$V_{\text{dc}} = v_{\text{dc,lo}} + v_{\text{dc,up}}, \tag{1}$$

and the NP potential, which is defined as

$$v_n = (v_{\text{dc,lo}} - v_{\text{dc,up}})/2, \tag{2}$$

floats. Therefore, the inverter output voltage $\boldsymbol{v}_{\text{inv}}$, which is equal to the stator voltage $\boldsymbol{v}_s$, can be written as

$$\boldsymbol{v}_{\text{inv}} = \boldsymbol{v}_s = \frac{V_{\text{dc}}}{2}\,\widetilde{\boldsymbol{K}}\,\boldsymbol{u}_{abc} - v_n\,\widetilde{\boldsymbol{K}}\,|\boldsymbol{u}_{abc}|, \tag{3}$$

where $\boldsymbol{u}_{abc} = [u_a\ u_b\ u_c]^T$ is the three-phase switch position, with $u_x \in \mathcal{U} = \{-1, 0, 1\}$, $x \in \{a, b, c\}$, being the single-phase switch position. Moreover, $|\boldsymbol{u}_{abc}| = [|u_a|\ |u_b|\ |u_c|]^T$ denotes the component-wise absolute value of $\boldsymbol{u}_{abc}$.

Since the currents at the NP sum up to zero, with the help of (2) the dynamics of the NP potential are captured in the expression

$$\frac{\mathrm{d}v_n}{\mathrm{d}t} = -\frac{i_n}{2X_{\text{dc}}}, \tag{4}$$

where the NP current i_n is the sum of the stator phase currents i_{sa}, i_{sb}, i_{sc}. Since the latter flow through the NP when the switch position of the corresponding phase is zero, the following holds

$$\begin{aligned} i_n = (1-|u_a|)i_{sa} + (1-|u_b|)i_{sb} + (1-|u_c|)i_{sc} \\ = -|\boldsymbol{u}_{abc}|^T \boldsymbol{i}_{s,abc}, \end{aligned} \tag{5}$$

where $\boldsymbol{i}_{s,abc} = [i_{sa}\ i_{sb}\ i_{sc}]^T$. Note that a star connection for the load is assumed in (5), i.e., $i_{sa} + i_{sb} + i_{sc} = 0$. Inserting (5) into (4) yields the final expression for the NP potential evolution

$$\frac{\mathrm{d}v_n}{\mathrm{d}t} = \frac{|\boldsymbol{u}_{abc}|^T \boldsymbol{i}_{s,abc}}{2X_{\text{dc}}}. \tag{6}$$

In direct MPC methods the dynamics of IM are typically modeled using the equivalent T-model [22, Chapter 2.2]. The latter, however, can be transformed into the simpler inverse-Γ model in Fig. 2 without any loss of information or accuracy [23]. In the equivalent circuit in Fig. 2 R_s and $\bar{R}_r$ are the stator and rotor resistances, respectively, $\bar{X}_m$ and X_σ are the mutual and total leakage reactances, $\bar{\boldsymbol{\psi}}_r$ and $\bar{\boldsymbol{i}}_r$ are the rotor flux and current, and ω_r is the angular rotor speed. Note that the overline in the listed machine parameters denotes the variables in the inverse-Γ model, which are defined in Appendix A.[1] The primary reason behind employing the discussed IM formulation can be understood by noting that the total leakage reactance

$$X_\sigma = (X_{ls} + X_m) - X_m^2/(X_{lr} + X_m) \tag{7}$$

includes both the stator X_{ls} and rotor X_{lr} leakage reactances of the machine, thus capturing their impact on the system model deviations. This facilitates the adoption of the estimation algorithm, as will be shown in Section IV.

To devise the prediction model of the drive, the switch position $\boldsymbol{u}_{abc} \in \boldsymbol{\mathcal{U}} = \mathcal{U}^3$ is defined as the system input, the stator current $\boldsymbol{i}_s$ and flux $\boldsymbol{\psi}_s$ together with the NP potential v_n are assigned to the state vector $\boldsymbol{x} = [\boldsymbol{i}_s^T\ \boldsymbol{\psi}_s^T\ v_n]^T \in \mathbb{R}^5$, while $\boldsymbol{i}_s$ and v_n are also considered as the system output

[1]For more details on the inverse-Γ model derivation and its comparison to the T-model the reader is referred to [13, Section II].

$\boldsymbol{y} = [\boldsymbol{i}_s^T \ v_n]^T \in \mathbb{R}^3$. In the next step the continuous-time state-space model is derived based on the circuit in Fig. 2

$$\frac{\mathrm{d}\boldsymbol{x}(t)}{\mathrm{d}t} = \mathbf{F}(t)\boldsymbol{x}(t) + \mathbf{G}\boldsymbol{u}_{abc}(t) \tag{8a}$$

$$\boldsymbol{y}(t) = \mathbf{C}\boldsymbol{x}(t), \tag{8b}$$

where the matrices $\mathbf{F}(t) \in \mathbb{R}^{5\times5}$, $\mathbf{G} \in \mathbb{R}^{5\times3}$, and $\mathbf{C} \in \mathbb{R}^{3\times5}$ are given in Appendix B. It is worth noting that $\mathbf{F}(t)$ contains multiplication of the input and the state, what makes the model nonlinear and poses challenges for the controller design. Following, (8) is discretized by adopting the forward Euler method with the sampling interval T_s

$$\boldsymbol{x}(k+1) = \mathbf{A}(k)\boldsymbol{x}(k) + \mathbf{B}\boldsymbol{u}_{abc}(k) \tag{9a}$$

$$\boldsymbol{y}(k) = \mathbf{C}\boldsymbol{x}(k)\,, \tag{9b}$$

where $\mathbf{A}(k) = \boldsymbol{I}_5 + \mathbf{F}(t)T_s$, $\mathbf{B} = \mathbf{G}T_s$, and $k \in \mathbb{N}$ denotes the discrete time step.

III. Controller Design

For the MV system in consideration the ultimate goal of the controller is to minimize the stator current distortions while keeping deviations of the NP potential and the switching power losses low. This is translated into the two sub-tasks of regulating the stator current $\boldsymbol{i}_s$ together with NP potential v_n along their references and minimizing the device switching frequency f_{sw}. For a one-step FCS-MPC the former objective is captured by the predicted output error $\boldsymbol{y}_{\mathrm{err}}(k+1) = \boldsymbol{y}_{\mathrm{ref}}(k+1) - \boldsymbol{y}(k+1)$, while the latter by the control effort $\Delta\boldsymbol{u}_{abc}(k) = \boldsymbol{u}_{abc}(k) - \boldsymbol{u}_{abc}(k-1)$.

To obtain a long-horizon formulation of the control problem, this work adopts the concept of the horizon combination $N = \{N_p, N_c\}$, where N_p denotes the number of discrete time steps wherein the system output behavior is predicted using (9), and N_c denotes the number of steps for which the possible switch positions are evaluated [13]. The discussed FCS-MPC design considerations can be captured by the following objective function

$$J = \sum_{\ell=k}^{k+N_p-1} \|\boldsymbol{y}_{\mathrm{err}}(\ell+1)\|_{\boldsymbol{Q}}^2 \ + \ \lambda_u \sum_{\ell=k}^{k+N_c-1} \|\Delta\boldsymbol{u}_{abc}(\ell)\|_2^2\,, \tag{10}$$

where the diagonal weighting matrix $\boldsymbol{Q} = \mathrm{diag}(1, 1, \lambda_n) \in \mathbb{R}^{3\times3}$ penalizes the deviation of the output variables from their references, and the weighting factors $\lambda_n, \lambda_u > 0$ set the trade-off between the stator current distortions, the NP voltage potential, and the switching frequency.

The task of the controller is to find the optimal sequence of control actions

$$\boldsymbol{U}^*(k) = \left[\boldsymbol{u}_{abc}^{*T}(k) \ \boldsymbol{u}_{abc}^{*T}(k{+}1) \ \ldots \ \boldsymbol{u}_{abc}^{*T}(k+N_c-1)\right]^T$$

by solving the following optimization problem

$$\underset{\boldsymbol{U}(k)\,\in\,\mathbb{U}}{\text{minimize}}\ J(k) \tag{11a}$$

$$\text{subject to} \tag{11b}$$

$$\boldsymbol{x}(j+1) = \mathbf{A}(j)\boldsymbol{x}(j) + \mathbf{B}\boldsymbol{u}_{abc}(j) \tag{11c}$$

$$\boldsymbol{y}(j+1) = \mathbf{C}\boldsymbol{x}(j+1), \forall j = k, \ldots, k{+}N_p{-}1 \tag{11d}$$

$$\|\Delta\boldsymbol{u}_{abc}(\ell)\|_\infty \leq 1, \qquad \forall \ell = k, \ldots, k{+}N_c{-}1, \tag{11e}$$

where $\mathbb{U} = \boldsymbol{\mathcal{U}} \times \cdots \times \boldsymbol{\mathcal{U}}$ is the $3N_c$-times Cartesian product of the set $\boldsymbol{\mathcal{U}}$, and represents the feasible input set.

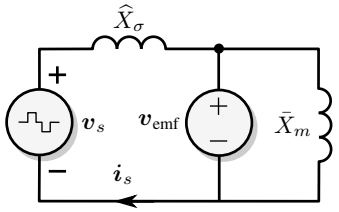

Fig. 3. Simplified equivalent model of an IM for the total leakage reactance estimation.

A common approach to solve (11) is the exhaustive search that evaluates all possible solutions, i.e., 3^{3N_c}, to conclude to the one that results in the minimum value of (10). Notably, the computational complexity of such an approach quickly exceeds the capabilities of modern control platforms. However, as was shown in [13], [21], the feature of long-horizon MPC strategies to predict the system evolution over a wider time window can be exploited at a marginal computational cost. Specifically, if operation at a low switching frequency range is considered, and thus the minimum amount of changes in the switch position is anticipated within a prediction window, then calculation of (11) up to N_p steps can be redundant. Thus, by setting $N_c < N_p$ the performance benefits of long horizons can be fully harvested. In such a case—that is tailored for MV applications—the exhaustive search can be a viable choice for a real-time implementation.

IV. Estimator Design

As can be seen from (10) the controller relies on (9) to compute the system predictions and consequently find the optimal solution. Therefore, whenever the system matrices $\mathbf{A}(k)$ and $\mathbf{B}$ do not reflect the actual system under test the control may result in a subpar performance. In relation to this drawback, [24] explored the effect of machine parameter deviations on the IM drive performance controlled by FCS-MPC. The study showed that variations in the rotor X_{lr} and stator X_{ls} leakage reactances have the most prominent impact on the system behavior. Obtaining the actual values of both parameters separately using sophisticated identification techniques usually results in an unwanted increase of the calculation burden. Fortunately, the adopted inverse-Γ model incorporates the said parameters implicitly in X_σ, see Fig. 2 and (7). The latter can be found in a computationally efficient manner, as shown in [21]. In the sequel, a short overview of the estimation algorithm is presented with necessary modifications to account for the varying NP potential. For the detailed implementation the reader is referred to [21].

The estimation algorithm assumes a sinusoidal form of the back electromotive force (back-EMF) $\boldsymbol{v}_{\mathrm{emf}}$ and constant amplitude during one sampling interval T_s. Given a negligible value of the stator resistance R_s in MV machines, and based on the equivalent circuit in Fig. 3, the following holds

$$\widehat{X}_\sigma \frac{\mathrm{d}\boldsymbol{i}_s(t)}{\mathrm{d}t} = \boldsymbol{v}_s(t) - \boldsymbol{v}_{\mathrm{emf}}(t), \tag{12}$$

where $\widehat{X}_\sigma$ denotes the estimated value of the total leakage reactance. In contrast to cases where a zero value of the NP potential is assumed, the evolution of the latter needs to be taken into account when computing $\boldsymbol{v}_s$ in (12) with the help

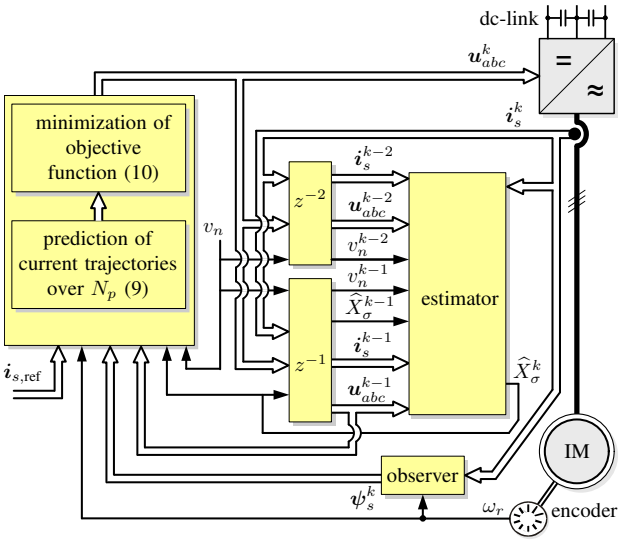

Fig. 4. Direct model predictive control with reference tracking and total leakage reactance estimator for MV VSD systems.

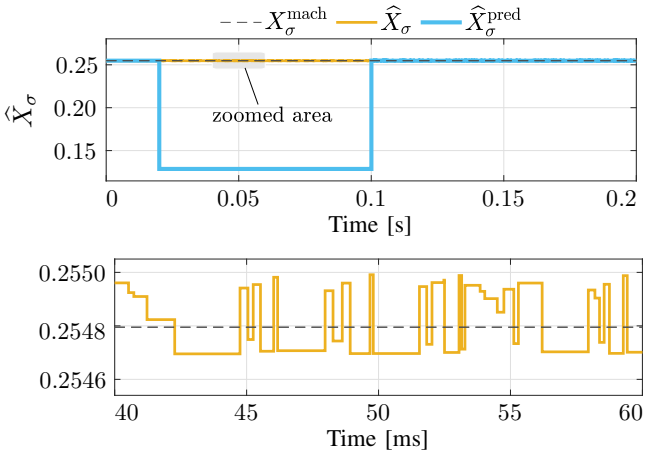

Fig. 5. Simulation results for estimation of the total leakage reactance X_σ (up) and its zoomed-in view (down).

of (3). Following, considering the assumptions above, $\widehat{X}_\sigma$ can be found by solving the quadratic equation

$$\widehat{X}_\sigma^2 A + \widehat{X}_\sigma B + C = 0\,, \tag{13}$$

where A, B, and C are defined in Appendix C.

The block diagram of the proposed FCS-MPC approach is shown in Fig. 4, while Fig. 5 demonstrates the effectiveness of the developed estimation algorithm. After simulating the drive operation with the nominal machine parameters $X_\sigma^{\text{pred}} = X_\sigma^{\text{mach}}$ for 20 ms a mismatch of -50% in both rotor X_{lr} and stator X_{ls} leakage reactances is introduced in the prediction model. This leads to the wrong leakage reactance $X_\sigma^{\text{pred}} = 0.13$ p.u. used by the proposed FCS-MPC. Next, at 0.1 s the prediction model starts to use the estimated value $X_\sigma^{\text{pred}} = \widehat{X}_\sigma$. It should be noted that the total leakage reactance is calculated throughout the whole simulation, and for the time period from 0 s to 0.1 s estimator runs in parallel to the control scheme.

V. Simulation Results

This section explores the time-domain results—presented in the p.u. system—for the proposed FCS-MPC. The setup under test is a three-level NPC inverter with a constant dc-link voltage of 5.2 kV and two dc-link capacitors of 2.24 mF each. The 2 MVA IM has rated voltage of 3.3 kV, and nominal stator frequency of 50 Hz, while its total leakage reactance is 0.25 p.u.[2] It is worth highlighting that the prediction model has a mismatch of $-50\,\%$ in the rotor X_{lr} and stator X_{ls} leakage reactances that is compensated for by the estimation algorithm. The controller sampling interval is $T_s = 25\,\mu$s, and the coefficient λ_u is chosen such that the resulting device switching frequency is $f_{\text{sw}} \approx 200$ Hz, while $\lambda_n = 5$. The system is tested with the horizon combination $N = \{5, 1\}$. According to [21, Section III], such a combination should deliver the optimal drive performance, i.e., the same as for $N = \{5, 5\}$, up to the critical switching frequency $f_{\text{sw}} = 666$ Hz. However, in case of $N = \{5, 1\}$ the associated computational effort facilitates the real-time implementation of the proposed FCS-MPC scheme, as the level of complexity of the optimization problem is similar to that of a one-step FCS-MPC, even though the prediction horizon is five steps.

Starting with the steady-state operation at nominal electromagnetic torque $T_e = 1$, Fig. 6 demonstrates the ability of the proposed scheme to accurately balance the NP potential along its reference $v_{n,\text{ref}} = 0$. Moreover, the stator currents follow their sinusoidal references. The stator current spectrum shows prominent odd non-triplen harmonics. In this regard, the results are similar to, e.g., synchronous optimal modulation that theoretically has the lowest possible current distortions for a given operating point [25]. Finally, the stator current THD value of $I_{\text{THD}} = 5.95\%$ and the stator current spectrum shape supports the statement of the improved drive performance in comparison to a one-step horizon. Namely, it can be seen that the said metrics are very close to ones in work [9], wherein FCS-MPC with $N = \{5, 5\}$ is implemented for an MV IM drive with effectively the same parameters.

As the next step, the transient operation is examined when the electromagnetic torque reference is stepped from 1 to 0 and vice versa at 5 ms and 20 ms, respectively. Notably, operating at zero torque is challenging for the NP potential control due to the 90° shift in phase between the stator phase voltages and currents [26]. Fig. 7 shows that in the presence of mismatches the NP potential is kept balanced along its reference during the transients. Furthermore, the scheme exhibits fast reference tracking, which is a typical characteristic of direct control methods. Specifically, T_e and $\boldsymbol{i}_{s,abc}$ settle at the new trajectories in a fraction of a millisecond at the step-down change in the torque reference. This is due to the available voltage margin in all the three phases at the moment of the commanded change. Note that, ensured by the controller design, the switching constraint is not violated. During the step-up change in T_e the transient takes about 3 ms limited only by the available voltage margin.

Finally, to highlight the active NP potential balancing ability of the proposed control scheme, Fig. 8 shows the effect of variations in λ_n. Specifically, when an initial offset v_n^{ini} is imposed, it is seen that with a higher penalization on v_n the NP potential is balanced faster.

[2]The complete list of the drive parameters can be found in [25, Table I].

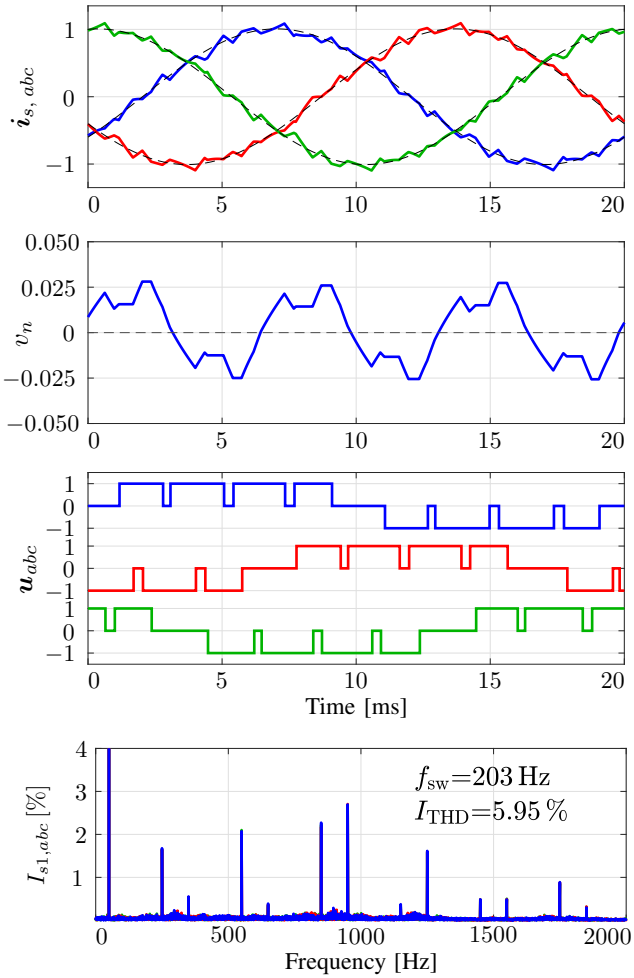

Fig. 6. Simulation results for the proposed FCS-MPC with $N = \{5, 1\}$ in steady state when a mismatch of -50% is simultaneously introduced in the rotor X_{lr} and stator X_{ls} leakage reactances, and the estimator is active.

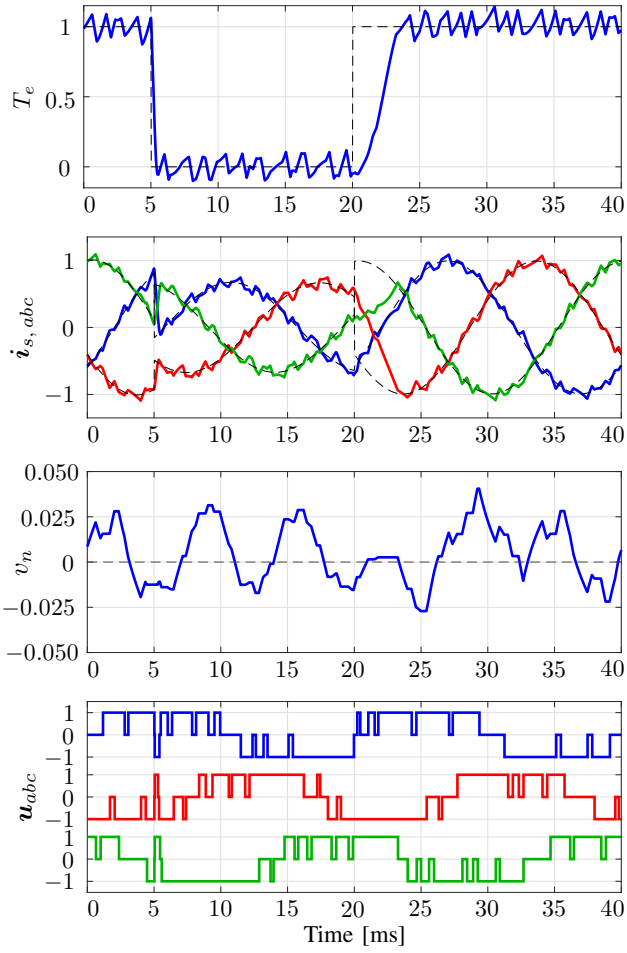

Fig. 7. Simulation results for the proposed FCS-MPC with $N = \{5, 1\}$ with steps in the electromagnetic torque reference when a mismatch of -50% is simultaneously introduced in the rotor X_{lr} and stator X_{ls} leakage reactances, and the estimator is active.

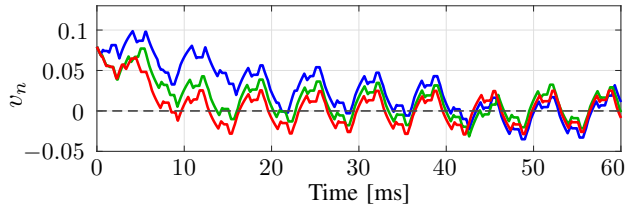

Fig. 8. Balancing of the NP potential v_n with the initial offset $v_n^{\mathrm{ini}} = 0.08$ p.u. for $\lambda_n = 1$ (blue line), $\lambda_n = 5$ (green line), and $\lambda_n = 15$ (red line). A mismatch of -50% is simultaneously introduced in the rotor X_{lr} and stator X_{ls} leakage reactances, and the estimator is active.

VI. Conclusion

The paper extended the algorithm proposed in [13] to include the balancing of the NP potential of a three-level NPC inverter driving an MV IM into the proposed FCS-MPC strategy. The method manages to control the stator currents along their references and balance the NP potential in a single control loop. Also the results indicate that the approach fully gains the performance benefits associated with long horizons and is robust to variations in the machine parameters. Thanks to the split prediction horizon and the light estimation algorithm, this is achieved with modest computational requirements, something that enables the real-time implementation of the proposed control strategy.

Appendix A
Variables of the Inverse-Γ Model

The parameters of the inverse-Γ model are defined with the help of the transformation coefficient $\gamma = X_m/(X_{lr} + X_m)$ as

$$\bar{\boldsymbol{i}}_r = \boldsymbol{i}_r/\gamma\,, \qquad \bar{X}_m = \gamma X_m\,,$$
$$\bar{\boldsymbol{\psi}}_r = \gamma\boldsymbol{\psi}_r\,, \qquad \bar{R}_r = \gamma^2 R_r\,.$$

Appendix B
System Matrices

$$\mathbf{F}(t) = \begin{bmatrix} \mathbf{F}_{\mathrm{IM}} & \begin{bmatrix} -\frac{1}{X_\sigma}\,\widetilde{\boldsymbol{K}}\,|\boldsymbol{u}_{abc}(t)| \\ -\,\widetilde{\boldsymbol{K}}\,|\boldsymbol{u}_{abc}(t)| \end{bmatrix} \\ \begin{bmatrix} \frac{1}{2X_{\mathrm{dc}}}|\boldsymbol{u}_{abc}(t)|^T\,\widetilde{\boldsymbol{K}}^{-1} & \mathbf{0}_{1\times 2} \end{bmatrix} & 0 \end{bmatrix}$$

$$\mathbf{F}_{\mathrm{IM}} = \begin{bmatrix} -\frac{1}{\tau_{s,\Gamma}} & -\omega_r & \frac{\bar{R}_r}{X_\sigma X_m} & \frac{\omega_r}{X_\sigma} \\ \omega_r & -\frac{1}{\tau_{s,\Gamma}} & -\frac{\omega_r}{X_\sigma} & \frac{\bar{R}_r}{X_\sigma X_m} \\ -R_s & 0 & 0 & 0 \\ 0 & -R_s & 0 & 0 \end{bmatrix},$$

where the transient stator time constant $\tau_{s,\Gamma}$ is given by

$$\frac{1}{\tau_{s,\Gamma}} = \frac{\bar{R}_r}{\bar{X}_m} + \frac{\bar{R}_r + R_s}{X_\sigma}\,.$$

$$\mathbf{G} = \frac{V_{\mathrm{dc}}}{2}\begin{bmatrix}\frac{1}{X_\sigma}\boldsymbol{I}_2 & \boldsymbol{I}_2 & \mathbf{0}_{2\times 1}\end{bmatrix}^T \widetilde{\boldsymbol{K}}, \quad \mathbf{C} = \begin{bmatrix}\boldsymbol{I}_2 & \mathbf{0}_{2\times 3} \\ \mathbf{0}_{1\times 2} & 0\ 0\ 1\end{bmatrix}.$$

Appendix C
Coefficients of the Quadratic Equation

$$\begin{aligned}
A &= \Delta A_\alpha^2(k+1) + \Delta A_\beta^2(k+1) - \Delta A_\alpha^2(k) \\
&\quad - \Delta A_\beta^2(k)\,, \\
B &= 2\Big(\Delta A_\alpha(k+1)v_{s\alpha}(k) + \Delta A_\beta(k+1)v_{s\beta}(k) \\
&\quad - \Delta A_\alpha(k)v_{s\alpha}(k-1) - \Delta A_\beta(k)v_{s\beta}(k-1)\Big)\,, \\
C &= v_{s\alpha}^2(k) + v_{s\beta}^2(k) - v_{s\alpha}^2(k-1) - v_{s\beta}^2(k-1)\,.
\end{aligned}$$

References

[1] M. Schweizer, T. Friedli, and J. W. Kolar, "Comparative evaluation of advanced three-phase three-level inverter/converter topologies against two-level systems," *IEEE Trans. Ind. Electron.*, vol. 60, no. 12, pp. 5515–5527, Dec. 2013.

[2] J. Pou, J. Zaragoza, S. Ceballos, M. Saeedifard, and D. Boroyevich, "A carrier-based PWM strategy with zero-sequence voltage injection for a three-level neutral-point-clamped converter," *IEEE Trans. Power Electron.*, vol. 27, no. 2, pp. 642–651, Feb. 2012.

[3] J. Pou, R. Pindado, D. Boroyevich, and P. Rodriguez, "Evaluation of the low-frequency neutral-point voltage oscillations in the three-level inverter," *IEEE Trans. Ind. Electron.*, vol. 52, no. 6, pp. 1582–1588, Dec. 2005.

[4] A. Zorig, S. Barkat, and A. Sangwongwanich, "Neutral point voltage balancing control based on adjusting application times of redundant vectors for three-level NPC inverter," *IEEE J. Emerg. Sel. Topics Power Electron.*, vol. 10, no. 5, pp. 5604–5613, Oct. 2022.

[5] N. Celanovic and D. Boroyevich, "A comprehensive study of neutral-point voltage balancing problem in three-level neutral-point-clamped voltage source PWM inverters," *IEEE Trans. Power Electron.*, vol. 15, no. 2, pp. 242–249, Mar. 2000.

[6] J. Pou, R. Pindado, D. Boroyevich, and P. Rodriguez, "Limits of the neutral-point balance in back-to-back-connected three-level converters," *IEEE Trans. Power Electron.*, vol. 19, no. 3, pp. 722–731, May 2004.

[7] M. Marchesoni, P. Segarich, and E. Soressi, "A new control strategy for neutral-point-clamped active rectifiers," *IEEE Trans. Ind. Electron.*, vol. 52, no. 2, pp. 462–470, Apr. 2005.

[8] J. Shen, S. Schroder, B. Duro, and R. Roesner, "A neutral-point balancing controller for a three-level inverter with full power-factor range and low distortion," *IEEE Trans. Ind. Appl.*, vol. 49, no. 1, pp. 138–148, Jan. 2013.

[9] E. Liegmann, P. Karamanakos, T. Geyer, T. Mouton, and R. Kennel, "Long-horizon direct model predictive control with active balancing of the neutral point potential," in *Proc. IEEE Int. Symp. Pred. Control Elect. Drives Power Electron.*, Pilsen, Czech Republic, Sep. 2017, pp. 89–94.

[10] F. Grimm, Z. Zhang, F. Wang, and R. Kennel, "Multistep predictive control of three-level NPC converters using weak derivative linearization," in *Proc. Chin. Autom. Congr.*, Jinan, China, Oct. 2017, pp. 4672–4677.

[11] P. Karamanakos, T. Geyer, N. Oikonomou, F. D. Kieferndorf, and S. Manias, "Direct model predictive control: A review of strategies that achieve long prediction intervals for power electronics," *IEEE Ind. Electron. Mag.*, vol. 8, no. 1, pp. 32–43, Mar. 2014.

[12] S. Baltruweit, E. Liegmann, P. Karamanakos, and R. Kennel, "FPGA-implementation friendly long-horizon finite control set model predictive control for high-power electronic systems," in *Proc. IEEE Energy Convers. Congr. Expo. Asia*, Singapore, May 2021, pp. 1823–1828.

[13] A. Tregubov, P. Karamanakos, and L. Ortombina, "A computationally efficient robust direct model predictive control for medium voltage induction motor drives," in *Proc. IEEE Energy Convers. Congr. Expo.*, Vancouver, BC, Canada, Oct. 2021, pp. 4690–4697.

[14] T. Geyer and D. E. Quevedo, "Multistep finite control set model predictive control for power electronics," *IEEE Trans. Power Electron.*, vol. 29, no. 12, pp. 6836–6846, Dec. 2014.

[15] P. Karamanakos, T. Geyer, and R. Kennel, "A computationally efficient model predictive control strategy for linear systems with integer inputs," *IEEE Trans. Contr. Syst. Technol.*, vol. 24, no. 4, pp. 1463–1471, Jul. 2016.

[16] L. Yan, F. Wang, M. Dou, Z. Zhang, R. Kennel, and J. Rodriguez, "Active disturbance-rejection-based speed control in model predictive control for induction machines," *IEEE Trans. Ind. Electron.*, vol. 67, no. 4, pp. 2574–2584, Apr. 2020.

[17] L. Yan and X. Song, "Design and implementation of Luenberger model-based predictive torque control of induction machine for robustness improvement," *IEEE Trans. Power Electron.*, vol. 35, no. 3, pp. 2257–2262, Mar. 2020.

[18] O. Wallscheid and E. F. B. Ngoumtsa, "Investigation of disturbance observers for model predictive current control in electric drives," *IEEE Trans. Power Electron.*, vol. 35, no. 12, pp. 13 563–13 572, Dec. 2020.

[19] O. Lipcak and J. Bauer, "MRAS-based induction machine magnetizing inductance estimator with included effect of iron losses and load," *IEEE Access*, vol. 9, pp. 166 234–166 248, Dec. 2021.

[20] F. Tinazzi, P. G. Carlet, S. Bolognani, and M. Zigliotto, "Motor parameter-free predictive current control of synchronous motors by recursive least-square self-commissioning model," *IEEE Trans. Ind. Electron.*, vol. 67, no. 11, pp. 9093–9100, Nov. 2020.

[21] A. Tregubov, P. Karamanakos, and L. Ortombina, "Long-horizon robust direct model predictive control for medium-voltage induction motor drives with reduced computational complexity," *IEEE Trans. Ind. Appl.*, vol. 59, no. 2, pp. 1775–1787, Mar. 2023.

[22] T. Geyer, *Model Predictive Control of High Power Converters and Industrial Drives*. Chichester, UK: Wiley, 2016.

[23] G. Slemon, "Modelling of induction machines for electric drives," *IEEE Trans. Ind. Appl.*, vol. 25, no. 6, pp. 1126–1131, Dec. 1989.

[24] L. Ortombina, P. Karamanakos, and M. Zigliotto, "Robustness analysis of long-horizon direct model predictive control: Induction motor drives," in *Proc. IEEE Workshop on Control and Model. for Power Electron.*, Aalborg, Denmark, Nov. 2020, pp. 1–8.

[25] M. A. W. Begh, P. Karamanakos, and T. Geyer, "Gradient-based predictive pulse pattern control with active neutral point balancing for three-level inverter medium-voltage drives," in *Proc. IEEE Energy Convers. Congr. Expo.*, Detroit, MI, USA, Oct. 2022, pp. 1–8.

[26] T. Geyer and V. Spudic, "Model predictive pulse pattern control with integrated balancing of the neutral point potential," in *Proc. Eur. Power Electron. Conf.*, Genova, Italy, Sep. 2019, pp. 1–10.